

# Adaptive optoelectronic camouflage systems with designs inspired by cephalopod skins

Cunjiang Yu<sup>a</sup>, Yuhang Li<sup>b,c</sup>, Xun Zhang<sup>d</sup>, Xian Huang<sup>d</sup>, Viktor Malyarchuk<sup>d</sup>, Shuodao Wang<sup>d</sup>, Yan Shi<sup>b,e</sup>, Li Gao<sup>d</sup>, Yewang Su<sup>b</sup>, Yihui Zhang<sup>b</sup>, Hangxun Xu<sup>f</sup>, Roger T. Hanlon<sup>g,h</sup>, Yonggang Huang<sup>b</sup>, and John A. Rogers<sup>d,i,1</sup>

<sup>a</sup>Department of Mechanical Engineering, Department of Electrical and Computer Engineering, University of Houston, Houston, TX 77204; <sup>b</sup>Department of Civil and Environmental Engineering, Department of Mechanical Engineering, Center for Engineering and Health, and Skin Disease Research Center, Northwestern University, Evanston, IL 60208; <sup>c</sup>The Solid Mechanics Research Center, Beihang University, Beijing 100191, China; <sup>d</sup>Department of Materials Science and Engineering, University of Illinois at Urbana–Champaign, Urbana, IL 61801; <sup>e</sup>State Key Laboratory of Mechanics and Control of Mechanical Structures, Nanjing University of Aeronautics and Astronautics, Nanjing 210016, China; <sup>f</sup>Department of Polymer Science and Engineering, Chinese Academy of Sciences Key Laboratory of Soft Matter Chemistry, University of Science and Technology of China, Hefei 230026, China; <sup>g</sup>Marine Biological Laboratory, Woods Hole, MA 02543; <sup>h</sup>Department of Ecology and Evolutionary Biology, Brown University, Providence, RI 02912; and <sup>i</sup>Department of Electrical and Computer Engineering, Department of Chemistry, Department of Mechanical Science and Engineering, Frederick Seitz Materials Research Laboratory, and Beckman Institute for Advanced Science and Technology, University of Illinois at Urbana–Champaign, Urbana, IL 61801

Edited by David A. Weitz, Harvard University, Cambridge, MA, and approved July 30, 2014 (received for review June 5, 2014)

**Octopus, squid, cuttlefish, and other cephalopods exhibit exceptional capabilities for visually adapting to or differentiating from the coloration and texture of their surroundings, for the purpose of concealment, communication, predation, and reproduction. Long-standing interest in and emerging understanding of the underlying ultrastructure, physiological control, and photonic interactions has recently led to efforts in the construction of artificial systems that have key attributes found in the skins of these organisms. Despite several promising options in active materials for mimicking biological color tuning, existing routes to integrated systems do not include critical capabilities in distributed sensing and actuation. Research described here represents progress in this direction, demonstrated through the construction, experimental study, and computational modeling of materials, device elements, and integration schemes for cephalopod-inspired flexible sheets that can autonomously sense and adapt to the coloration of their surroundings. These systems combine high-performance, multiplexed arrays of actuators and photodetectors in laminated, multilayer configurations on flexible substrates, with overlaid arrangements of pixelated, color-changing elements. The concepts provide realistic routes to thin sheets that can be conformally wrapped onto solid objects to modulate their visual appearance, with potential relevance to consumer, industrial, and military applications.**

flexible electronics | metachrosis | thermochromic

Recently established understanding of many of the key organ and cellular level mechanisms of cephalopod metachrosis (1–5) creates opportunities for the development of engineered systems that adopt similar principles. Here, critical capabilities in distributed sensing and actuation (6–9) must be coupled with elements that provide tunable coloration, such as the thermochromic systems reported here or alternatives such as cholesteric liquid crystals (10–13), electrokinetic and electrofluidic structures (14, 15), or colloidal crystals (16–19). Although interactive displays that incorporate distributed sensors for advanced touch interfaces (20–22) might have some relevance, such capabilities have not been explored in flexible systems or in designs that enable adaptive camouflage. The results reported here show that advances in heterogeneous integration and high-performance flexible/stretchable electronics provide a solution to these critical subsystems when exploited in thin multilayer, multifunctional assemblies. The findings encompass a complete set of materials, components, and integration schemes that enable adaptive optoelectronic camouflage sheets with designs that capture key features and functional capabilities of the skins of cephalopods. These systems combine semiconductor actuators, switching components, and light sensors with inorganic reflectors and organic color-changing materials in a way that allows autonomous

matching to background coloration, through the well-known, separate working principles of each component. The multilayer configuration and the lamination processes used for assembly, along with the photopatternable thermochromic materials, are key to realization of these systems. Demonstration devices capable of producing black-and-white patterns that spontaneously match those of the surroundings, without user input or external measurement, involve multilayer architectures and ultrathin sheets of monocrystalline silicon in arrays of components for controlled, local Joule heating, photodetection, and two levels of matrix addressing, combined with metallic diffuse reflectors and simple thermochromic materials, all on soft, flexible substrates. Systematic experimental, computational, and analytical studies of the optical, electrical, thermal, and mechanical properties reveal the fundamental aspects of operation, and also provide quantitative design guidelines that are applicable to future embodiments.

The skin of a cephalopod enables rapid, patterned physiological color change, or metachrosis, in a thin three-layered system (2, 23–25). The topmost layer is pigmentary coloration: chromatophore organs that retract or expand rapidly by direct control of muscles that are in turn controlled by nerves originating in the brain. This physiological on/off speed change

## Significance

**Artificial systems that replicate functional attributes of the skins of cephalopods could offer capabilities in visual appearance modulation with potential utility in consumer, industrial, and military applications. Here we demonstrate a complete set of materials, components, fabrication approaches, integration schemes, bioinspired designs, and coordinated operational modes for adaptive optoelectronic camouflage sheets. These devices are capable of producing black-and-white patterns that spontaneously match those of the surroundings, without user input or external measurement. Systematic experimental, computational, and analytical studies of the optical, electrical, thermal, and mechanical properties reveal the fundamental aspects of operation and also provide quantitative design guidelines that are applicable to future embodiments.**

Author contributions: C.Y. and J.A.R. designed research; C.Y., Y.L., X.Z., X.H., V.M., S.W., Y. Shi, L.G., Y. Su, Y.Z., H.X., Y.H., and J.A.R. performed research; C.Y., Y.L., Y. Su, Y.Z., Y.H., and J.A.R. analyzed data; and C.Y., Y.L., Y. Shi, Y. Su, R.T.H., Y.H., and J.A.R. wrote the paper.

The authors declare no conflict of interest.

This article is a PNAS Direct Submission.

<sup>1</sup>To whom correspondence should be addressed. Email: jrogers@illinois.edu.

This article contains supporting information online at [www.pnas.org/lookup/suppl/doi:10.1073/pnas.1410494111/-DCSupplemental](http://www.pnas.org/lookup/suppl/doi:10.1073/pnas.1410494111/-DCSupplemental).





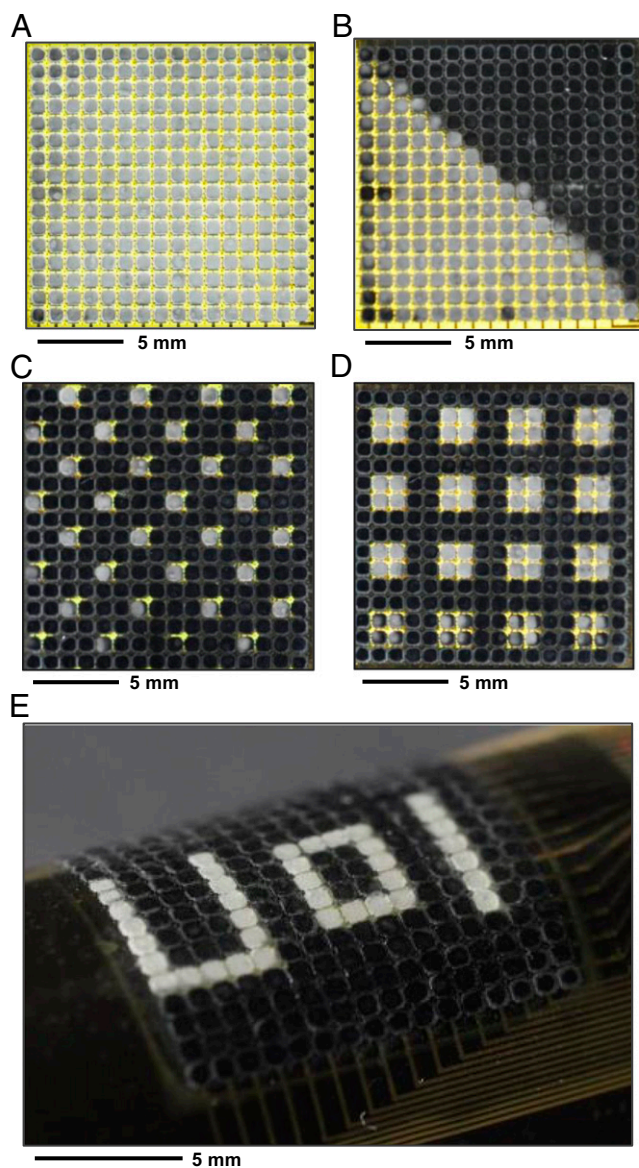


**Fig. 3.** Illustration of metachrosis for several different static patterns. Top view image of the device in a uniform geometry (A), in a triangular pattern (B), and in an array of small (C) and large (D) squares. (E) Image of a device in operation while bent, while showing the text pattern “U o l”.

This color changing strategy offers viewing-angle-independent appearance and a simple, thermal switching mechanism, suitable for present demonstration purposes. The high thermal conductivity of the Ag layer is important for this latter feature, as described subsequently.

Selective actuation of these photodefined chromatophores/leucophores yields programmable patterns of black and white. An array of ultrathin (total thickness  $\sim 10$   $\mu\text{m}$ ; bending stiffness per length  $\sim 1.7$   $\mu\text{N}$ ) Si diodes (single crystal Si  $640 \times 640$   $\mu\text{m}^2$  in area,  $1.25$   $\mu\text{m}$  thick) provides local heating for this purpose, with multiplexed addressing (*SI Appendix*, Fig. S2). Details of the fabrication and optical images of representative devices appear in *SI Appendix*, Figs. S3, S4, and S2C, respectively. The yields are  $>95\%$ . Fig. 2B presents the current-voltage (I-V) characteristics of a typical device (forward voltage  $\sim 0.7$  V; current  $\sim 190$  mA at a forward bias of 10.5 V). The properties are independent of temperature over this range, thereby ensuring stable behavior

in all relevant operating modes presented here. Multiplexed addressing involves application of power in a pulsed mode, with row/column scanning. The designs of the external electronics for this purpose are summarized in *SI Appendix*, Figs. S5 and S6. The ability to localize heating to a single unit cell in this manner is demonstrated in *SI Appendix*, Fig. S2D.

Distributed sensing of background patterns is achieved via artificial opsins that consist of photodiodes and multiplexing switches. The materials and fabrication schemes for these components are similar to those of the Joule heating elements described above. (Details appear in *SI Appendix*.) The responses of the photodetectors define the pattern of thermal actuation and, therefore, the resulting patterns of coloration. As illustrated in Fig. 1E and *SI Appendix*, Fig. S7A and B, each unit cell includes a photodiode and a multiplexing (blocking) diode connected in a back-to-back fashion. These devices are positioned at the notches in the patterned chromatophore/leucophore pixels to allow exposure to light incident on the system from above or below. The blocking diode incorporates an opaque coating to eliminate its sensitivity to light. The I-V curves of the photodetector in dark and light conditions appear in Fig. 2C, where the dark current is  $\sim 1$  nA and the photocurrent is  $\sim 1$   $\mu\text{A}$ . The yields are  $\sim 100\%$ . A digital image that results from patterned illumination appears in *SI Appendix*, Fig. S8A and B. A binarized intensity distribution derived from such an image serves as a control signal to establish closed-loop operation of the entire system. The actuation and sensing layers have excellent flexibility (*SI Appendix*, Figs. S4D and S7C) due to their thin construction. No delamination occurs even when the integrated device was bent to a radius of 2 mm. Finite element modeling (FEM) results for bending to this degree appear in *SI Appendix*, Fig. S12A. The same geometry allows separate fabrication of these layers and subsequent lamination of them on top of one another to form a complete system (*SI Appendix*, Fig. S9). The lamination process occurs at the wafer scale, with the potential for use over larger areas with proper tooling and alignment procedures. This type of integration allows separate fabrication of the various subsystems, thereby improving the overall device yields, to levels of  $>95\%$ . Images of the device before and after integrating the Ag layers are shown in *SI Appendix*, Fig. S10A and B. Thin flexible cables based on anisotropic conductive films bond to electrode pads at the periphery for electrical connection to external power supply and analysis hardware, as in *SI Appendix*, Fig. S11.

Multiplexed photodetection and coordinated actuation are central to the overall operation. Responses of the diodes under pulsed mode voltages between 5.5 V and 12.5 V yield insights into the mechanisms of heating and thermal diffusion. Measurements under these conditions involve digital image capture of color changes in the chromatophore, simultaneously with temperature evaluation using an infrared (IR) camera (A655SC, FLIR Systems, Inc.). The minimum operating voltage is defined by initiation of color change at the location of the targeted pixel; the maximum is defined by onset of change in adjacent pixels, via thermal diffusion. As shown in *SI Appendix*, Figs. S13 and S14, typical minimum and maximum voltages are  $\sim 10.5$  V and  $\sim 11.5$  V, respectively. All system tests reported here used values near the minimum. Fig. 2D illustrates measured (top) and computed (bottom) distributions of temperature during operation of a single, isolated pixel. The multiplexing scheme naturally leads to fluctuations in temperature about a baseline level, as shown in the experimental (black dots) and 3D FEM results (red lines) of Fig. 2E and F, and *SI Appendix*, Fig. S15. Here, the applied power begins and ends at 11 s and 41 s, respectively. The pulses have a duration of  $t_0 = 17.5$  ms and a period of  $T = 280$  ms. The color changes from white to black after  $\sim 1$  s, corresponding to four pulses. Results of *SI Appendix*, Fig. S15B, indicate that the temperature increases sharply and then fluctuates between  $47^\circ\text{C}$  and  $60^\circ\text{C}$ , after stabilization. A key finding is that changes in

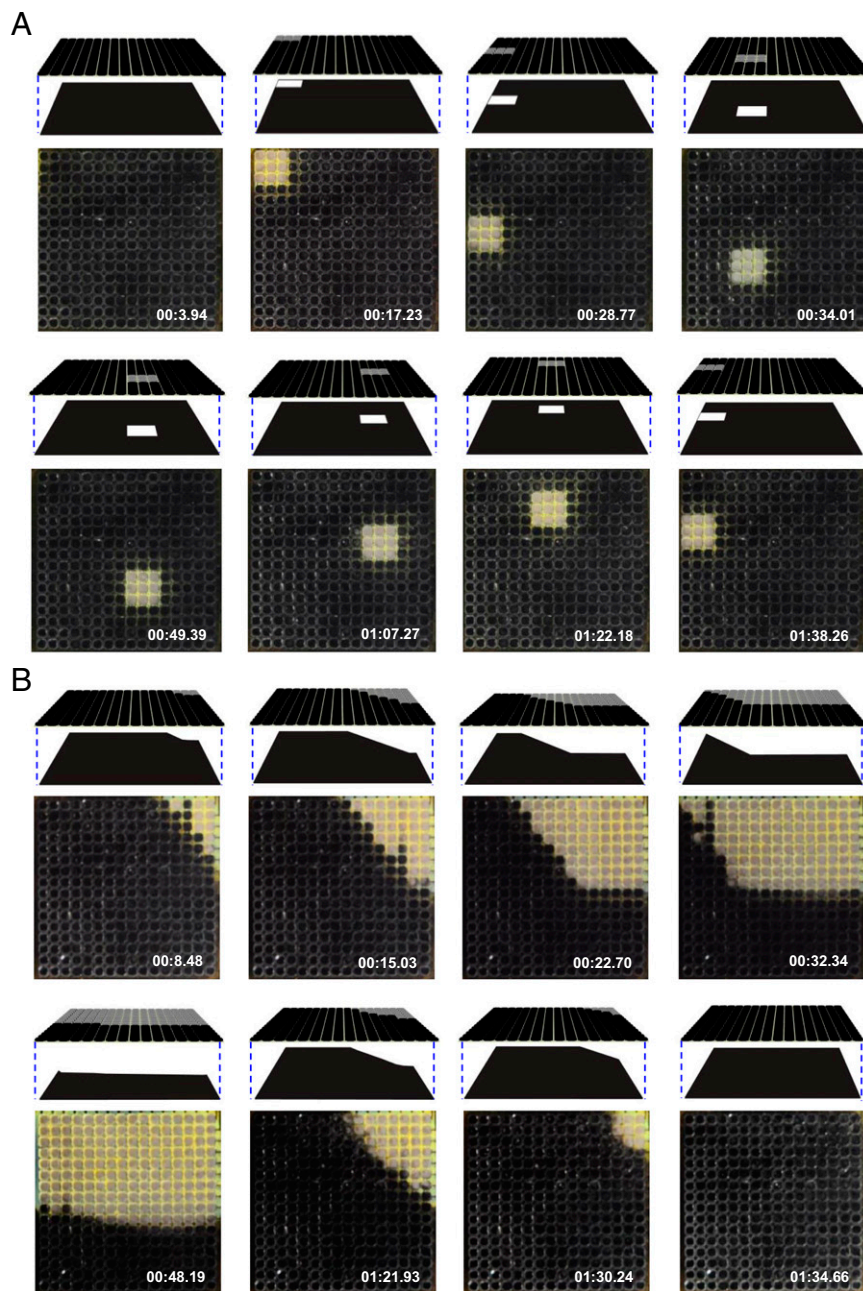


**Fig. 4.** Two demonstrations of autonomous, dynamic metachrosis. (A) Sequence of images extracted from a movie (time stamp in the lower right) that demonstrates adaptive pattern matching to a continuously changing background, created in this case by moving a mask that allows passage of light through a square region. At the top are angled view schematic illustrations of the experiment (top: device; bottom: pattern background). (B) Results similar to those in A, but obtained with a different mask geometry.

temperature remain confined largely to a single pixel, without significant diffusion to neighboring pixels (*SI Appendix, Fig. S17*). The lateral uniformity and pixel-level localization of the changes in temperature follow from (i) the high thermal conductivity of the Ag layer and its ability to facilitate thermal diffusion from the diode source (*SI Appendix, Fig. S20*) and (ii) the pixelated pattern of this material and the leucodye composite. The temperature (see *SI Appendix, Fig. S18*) is nearly constant throughout the depth of this composite (see *SI Appendix, Fig. S19*), due to its thin geometry. These collective features enable arbitrary pattern generation to a resolution set by the numbers of pixels and their sizes. An example of a pattern of the character

“O” appears in [Movie S1](#) (experimental results) and [Movie S2](#) (modeling results).

Experimental procedures used to study camouflage capabilities in cuttlefish (2, 30–33) serve as a model for illustrating full function, i.e., metachrosis, of the systems. Here, a device rests on a patterned black-and-white background formed by passing white light through an amplitude mask from below. External control electronics automatically send signals to the actuators at locations where responses from associated photo-detectors exceed a threshold. Fig. 3A shows a case in which all pixels turn white, consistent with the uniformly bright pattern of the background. Different static geometries, including triangles,

arrays of dots, and even random patterns, can be achieved, with either flat or curved configurations, as shown in Fig. 3 B–E.

Dynamic pattern recognition and matching are also possible, as illustrated in Fig. 4 A and B. In this case, changing the position of an amplitude mask that passes light only through a small square region leads to corresponding changes in the displayed patterns (Fig. 4A). In these images and others of Fig. 4, the top illustrations correspond to schematic, angled view renderings of the mask and the device; the images directly below are top views of the device. Movies S3 and S4 show additional details and examples. The metachrosis process occurs within 1 or 2 s in all cases, which is similar to neutrally controlled pattern change in cephalopods (2).

## Discussion

These systems establish foundations in materials science and engineering design that address key challenges in distributed sensing, actuation, and control in adaptive camouflage. The sensors and actuators provide operation across the full visible spectrum and allow for electric-field- or current-induced switching, respectively. As a result, these ideas can be applied not only with simple thermochromic materials but also with more advanced alternatives that offer improved power efficiency, facile routes to color, and robust operation without sensitivity to environmental conditions. Furthermore, the overall architecture can accommodate integration of tunable analogs to iridophores, thereby providing a vehicle for future investigations. In all cases, compatibility with large-area electronics holds promise for scalable manufacturing. Ability to reproduce physical texture, as in many cephalopods (34), remains as an interesting and challenging topic for research.

## Materials and Methods

**Fabrication and Assembly.** Detailed fabrication procedures for the various individual components of the system appear in *SI Appendix*. The assembly

process involves a series of lamination processes. First, a slab of PDMS (Sylgard 184, Dow Corning) was used to retrieve an interconnected array of multiplexed silicon diodes after release from a glass substrate. Exposing a separate layer of PDMS (100  $\mu\text{m}$ , on a glass substrate) to UV-induced ozone (BHK, Inc.) generated a hydroxyl-terminated surface for bonding via condensation reactions with similar chemistry associated with a layer  $\text{SiO}_2$  blanket deposited onto the array. The Ag (thickness 300 nm) and the thermochromic composite (thickness  $\sim 65 \mu\text{m}$ ) were lithographically patterned on top of the diode array. Alignment followed a scheme shown in *SI Appendix*, Fig. S10C. The resulting system, with the PDMS layer, was then peeled from the glass. Similar bonding processes enabled aligned integration of a separately fabricated multiplexed array of photodetectors onto the backside of the PDMS, through the use of modified mask aligner (MJB-3, Karl Suss) with alignment accuracy of 1  $\mu\text{m}$ . Details appear in *SI Appendix*, *Fabrication and assembling the complete system and Fig. S9*.

**Control and System Operation.** The system consists of two sets of active components, i.e., sensors and actuators, each of which functions separately and at different multiplexed scanning speeds. Closed-loop operation involves (i) acquiring digital images based on the intensity distributions extracted from responses of the  $16 \times 16$  array of photodetectors, (ii) binarizing the intensity distribution and storing the resulting data in a buffer, and (iii) reading the buffer and addressing the  $16 \times 16$  array of actuators by column scanning to copy the pattern, in a repeating manner. The time to acquire an image is  $\sim 10$  ms, much shorter than the pulse period for actuation (280 ms), thereby ensuring that the refresh rate of the image exceeds that of induced color change. Software development tools from LabVIEW 2012 provide all of the necessary means for implementation of the described operation.

**ACKNOWLEDGMENTS.** Jeff Grau is acknowledged for his help in preparing photomasks. The work on material design and device fabrication was supported by Office of Naval Research under Grant N00014-10-1-0989. C.Y. acknowledges the start-up funding support from the Department of Mechanical Engineering, Cullen College of Engineering, and the Division of Research at the University of Houston. R.T.H. also acknowledges partial support from Air Force Office of Scientific Research Grant FA9550-09-0346.

- Mäthger LM, Denton EJ, Marshall NJ, Hanlon RT (2009) Mechanisms and behavioural functions of structural coloration in cephalopods. *J R Soc Interface* 6(Suppl 2): S149–S163.
- Hanlon RT (2007) Cephalopod dynamic camouflage. *Curr Biol* 17(11):R400–R404.
- Hanlon RT, et al. (2009) Cephalopod dynamic camouflage: Bridging the continuum between background matching and disruptive coloration. *Philos Trans R Soc Lond B Biol Sci* 364(1516):429–437.
- Messenger JB (2001) Cephalopod chromatophores: Neurobiology and natural history. *Biol Rev Camb Philos Soc* 76(4):473–528.
- Hanlon RT (1982) The functional-organization of chromatophores and iridescent cells in the body patterning of *Loligo-plei* (Cephalopoda, Myopsida). *Malacologia* 23(1):89–119.
- Manakasettharn S, Taylor JA, Krupenkin TN (2011) Bio-inspired artificial iridophores based on capillary origami: Fabrication and device characterization. *Appl Phys Lett* 99(14):144102.
- Morin SA, et al. (2012) Camouflage and display for soft machines. *Science* 337(6096): 828–832.
- Rossiter J, Yap B, Conn A (2012) Biomimetic chromatophores for camouflage and soft active surfaces. *Bioinspir Biomim* 7(3):036009.
- Phan L, et al. (2013) Reconfigurable infrared camouflage coatings from a cephalopod protein. *Adv Mater* 25(39):5621–5625.
- Coles HJ, Pivnenko MN (2005) Liquid crystal ‘blue phases’ with a wide temperature range. *Nature* 436(7053):997–1000.
- Kahn FJ (1970) Electric-field-induced color changes and pitch dilation in cholesteric liquid crystals. *Phys Rev Lett* 24(5):209–212.
- Kikuchi H, Yokota M, Hisakado Y, Yang H, Kajiyama T (2002) Polymer-stabilized liquid crystal blue phases. *Nat Mater* 1(1):64–68.
- Sackmann E (1971) Photochemically induced reversible color changes in cholesteric liquid crystals. *J Am Chem Soc* 93(25):7088–7090.
- Comiskey B, Albert JD, Yoshizawa H, Jacobson J (1998) An electrophoretic ink for all-printed reflective electronic displays. *Nature* 394(6690):253–255.
- Heikenfeld J, et al. (2009) Electrofluidic displays using Young–Laplace transposition of brilliant pigment dispersions. *Nat Photonics* 3(5):292–296.
- Vukusic P, Sambles JR (2003) Photonic structures in biology. *Nature* 424(6950): 852–855.
- Arsenault AC, et al. (2006) From colour fingerprinting to the control of photoluminescence in elastic photonic crystals. *Nat Mater* 5(3):179–184.
- Harun-Ur-Rashid M, Seki T, Takeoka Y (2009) Structural colored gels for tunable soft photonic crystals. *Chem Rec* 9(2):87–105.
- Kim H, et al. (2009) Structural colour printing using a magnetically tunable and lithographically fixable photonic crystal. *Nat Photonics* 3(9):534–540.
- Wang C, et al. (2013) User-interactive electronic skin for instantaneous pressure visualization. *Nat Mater* 12(10):899–904.
- Boer W, Abileah A (2005) US Patent 6,947,102 B2.
- Choi J, Joo I, Kim H (2010) US Patent 7,800,602 B2.
- Kreit E, et al. (2012) Biological versus electronic adaptive coloration: How can one inform the other? *J R Soc Interface* 10(78):20120601.
- Mäthger LM, Hanlon RT (2007) Malleable skin coloration in cephalopods: Selective reflectance, transmission and absorbance of light by chromatophores and iridophores. *Cell Tissue Res* 329(1):179–186.
- Mathger LM, et al. (2013) Bright white scattering from protein spheres in color changing, flexible cuttlefish skin. *Adv Funct Mater* 23(32):3980–3989.
- Mäthger LM, Roberts SB, Hanlon RT (2010) Evidence for distributed light sensing in the skin of cuttlefish, *Sepia officinalis*. *Biol Lett* 6(5):600–603.
- Anonymous (2002) *Chemistry and Applications of Leuco Dyes* (Plenum, New York).
- Siegel AC, Phillips ST, Wiley BJ, Whitesides GM (2009) Thin, lightweight, foldable thermochromic displays on paper. *Lab Chip* 9(19):2775–2781.
- Yu C, et al. (2014) All-elastomeric, strain-responsive thermochromic color indicators. *Small* 10(7):1266–1271.
- Forsythe JW, Hanlon RT (1988) Behavior, body patterning and reproductive biology of *Octopus bimaculoides* from California. *Malacologia* 29(1):41–55.
- Hanlon RT, Messenger JB (1988) Adaptive coloration in young cuttlefish (*Sepia officinalis* l) - the morphology and development of body patterns and their relation to behavior. *Philos Trans R Soc Lond B Biol Sci* 320(1200):437–487.
- Mäthger LM, et al. (2007) Disruptive coloration elicited on controlled natural substrates in cuttlefish, *Sepia officinalis*. *J Exp Biol* 210(Pt 15):2657–2666.
- Zylinski S, Osorio D, Shohet AJ (2009) Cuttlefish camouflage: Context-dependent body pattern use during motion. *Proc R Soc B* 276(1675):3963–3969.
- Allen JJ, Bell GRR, Kuzirian AM, Velankar SS, Hanlon RT (2014) Comparative morphology of changeable skin papillae in octopus and cuttlefish. *J Morphol* 275(4): 371–390.

Supporting Information

**Adaptive optoelectronic camouflage systems with designs inspired by cephalopod skins**

Cunjiang Yu<sup>a</sup>, Yuhang Li<sup>b,c</sup>, Xun Zhang<sup>d</sup>, Xian Huang<sup>d</sup>, Viktor Malyarchuk<sup>d</sup>, Shuodao Wang<sup>d</sup>, Yan Shi<sup>b,e</sup>, Li Gao<sup>d</sup>, Yewang Su<sup>b</sup>, Yihui Zhang<sup>b</sup>, Hangxun Xu<sup>f</sup>, Roger Hanlon<sup>g,h</sup>, Yonggang Huang<sup>b</sup>, and John A. Rogers<sup>d,i,1</sup>

<sup>a</sup>*Department of Mechanical Engineering, Department of Electrical and Computer Engineering, University of Houston, Houston, TX 77204*

<sup>b</sup>*Department of Civil and Environmental Engineering, Department of Mechanical Engineering, Center for Engineering and Health, and Skin Disease Research Center, Northwestern University, Evanston, IL 60208*

<sup>c</sup>*The Solid Mechanics Research Center, Beihang University, Beijing 100191, China*

<sup>d</sup>*Department of Materials Science and Engineering, University of Illinois at Urbana-Champaign, Urbana, IL 61801*

<sup>e</sup>*State Key Laboratory of Mechanics and Control of Mechanical Structures, Nanjing University of Aeronautics and Astronautics, Nanjing 210016, China*

<sup>f</sup>*Department of Polymer Science and Engineering, CAS Key Laboratory of Soft Matter Chemistry, University of Science and Technology of China, Hefei 230026, China*

<sup>g</sup>*Marine Biological Laboratory, Woods Hole, MA, 02543*

<sup>h</sup>*Department of Ecology and Evolutionary Biology, Brown University, Providence, RI, 02912*

<sup>i</sup>*Department of Electrical and Computer Engineering, Department of Chemistry, Department of Mechanical Science and Engineering, Frederick-Seitz Materials Research Laboratory, and Beckman Institute for Advanced Science and Technology, University of Illinois at Urbana-Champaign, Urbana, IL 61801*

<sup>1</sup>*To whom correspondence should be addressed. E-mail: jrogers@illinois.edu.*

## **1. Preparing the thermochromic composite and measuring its optical characteristics**

Preparation of the photodefinable thermochromic composite involved mixing microencapsulated leuco dye (black 47C, LCR Hallcrest) with SU-8 50 (Microchem, USA) at a weight ratio of 1:5 to form a liquid slurry. Microcapsules contain mixtures of leuco dye with a color developer and a low melting point solvent. At low temperatures, the developer and leuco dye form a complex that favors a colored ring-open state. Upon heating, the solvent melts, and the developer and dye dissociate. In this state, the leuco dye favors a colorless, ring-closed configuration. Such transformation occurs at 47 °C in a reversible manner. Figure S1A shows an optical image of the slurry at 22 °C. Heating to a temperature above 47 °C causes the slurry to become transparent. As shown in Fig. S1B, a background picture underneath the slurry is clearly visible at temperatures above 47 °C. Standard procedures for patterning SU-8 yield pixelated arrays of this slurry with thickness defined by the spin-speed. Figures S1C and D provide SEM images of examples. Detailed fabrication steps appear below.

The optical reflectance of the color changeable pixels (Ag/composite dye) was measured using a spectrometer (Cary 5G UV-VIS-NIR) as a function of temperature. A portable thermoelectric heater/cooler (InbS1-031.021, WATRONIX, Inc.) served to control the sample temperature. A thermocouple (Fluke 233, Fluke Corporation) was used to measure the temperature.

### **Fabrication steps:**

1. Mix leuco dye and SU-8 50 at weight ratio of 1:5.
2. Spin-coat the mixture slurry (3000rpm, 30 sec).
3. Pre-bake at 65 °C for 5 min and 95 °C for 20 min.
4. Expose to UV light under a mask aligner (Karl Suss MJB3) at a dose of 1440 mJ/cm<sup>2</sup>.
5. Post-bake at 65 °C for 2 min and 95 °C for 5 min.

6. Develop in SU-8 developer (MicroChem, USA) for 6 minutes.
7. Rinse in isopropyl alcohol (IPA) and deionized (DI) water.

## **2. Fabricating the diode array and measuring its electrical characteristics**

Figure S2A shows an exploded schematic illustration of the layout of the Si, metal and polyimide (PI) layers associated with a single pixel in the heater array. The major steps in the fabrication include retrieving a thin (1.25  $\mu\text{m}$ ) crystalline film of Si with pre-defined patterns of doping from a silicon-on-insulator (SOI) wafer followed by transfer printing onto a thin polyimide (PI) substrate, and then applying layers for metallization and passivation, as outlined in Figs. S3 and 4. A thin layer of gold eliminates the potential for crosstalk induced by light. Figure S2B shows the planar structure and design of the Si heater; the small dots correspond to holes introduced into the Si to facilitate chemical etching for release. The measured I-V curves at different temperatures appear in Fig. 2B. Figure S2C shows an optical image of a  $16\times 16$  array of unit cells. Individual addressing is achieved without affecting the neighborhood pixels, as evidenced by the IR image (QFI InfraScope II) of Fig. S2D. Here, the background temperature was set to 30  $^{\circ}\text{C}$ , to facilitate IR imaging. Detailed fabrication steps are as follows.

### **Fabrication steps:**

#### ***Defining alignment markers***

1. Clean 1.25  $\mu\text{m}$  SOI wafer (acetone, isopropyl alcohol (IPA), deionized (DI) water).
2. Pattern photoresist (PR; Clariant AZ5214, 3000 rpm, 30 sec) with 365 nm optical lithography (Mask #1: Alignment marker).
3. Etch Si by RIE (50 mTorr, 40 sccm  $\text{SF}_6$ , 100 Watt, 1 min).
4. Remove PR by acetone and clean by piranha for 10 min.

#### ***Performing p+ doping***

5. Deposit 900 nm SiO<sub>2</sub> by plasma enhanced chemical vapor deposition (PECVD; PlasmaTherm SLR).
6. Treat with hexamethyldisilazane (HMDS) for 2 min.
7. Pattern PR (Mask #2: P doping).
8. Bake at 110°C for 5 min.
9. Etch SiO<sub>2</sub> in buffered oxide etchant (BOE, 6:1) for 1.5 min.
10. Remove PR by acetone and clean by piranha for 10 min.
11. Expose to a boron doping source at 1000°C for 30 min.
12. Clean the processed wafer (concentrated (49%) HF 2 min, piranha 10 min, BOE 1 min).

***Performing n+ doping***

13. Deposit 900 nm SiO<sub>2</sub> by PECVD.
14. Treat with HMDS for 2 min.
15. Pattern PR (Mask #3: N doping).
16. Bake at 110°C for 5 min.
17. Etch SiO<sub>2</sub> in buffered oxide etchant (BOE, 6:1) for 1.5 min.
18. Remove PR by acetone and clean by piranha for 10 min.
19. Expose to a phosphorus doping source at 1000°C for 10 min.
20. Clean the processed wafer (HF 2 min, piranha 10 min, BOE 1 min).

***Releasing the top Si from SOI***

21. Pattern PR (AZ 5214) (Mask #4: Releasing hole 1).
22. Etch Si by RIE (50 mTorr, 40 sccm SF<sub>6</sub>, 100 Watt, 3.5 min).
23. Remove PR by acetone and clean by piranha for 10 min.
24. Etch buried oxide layer in concentrated HF for 45 min.

25. Rinse and clean the processed wafer in DI wafer.

***Retrieving the Si film***

26. Bring a 6 mm thick PDMS (weight ratio of base: curing agent=10:1) stamp into contact with the Si.

27. Peel the stamp back to lift the Si film from SOI onto the stamp.

***Preparing the carrier wafer***

28. Spin cast polyimide (PI, poly(pyromellitic dianhydride-co-4,4'-oxydianiline) (4000 rpm, 30 sec) onto a 3"×2" glass slide.

29. Anneal at 150 °C for 10 min.

30. Anneal at 250 °C for 60 min in an N<sub>2</sub> atmosphere.

31. Deposit Cr/Au (5/300 nm) by electron beam evaporation (AJA International).

***Transfer printing the Si film***

32. Spin coat the carrier wafer with PI (4000 rpm, 30 sec).

33. Bake at 110 °C for 30 sec.

34. Bring the stamp with Si film on its surface into contact with the carrier wafer.

35. Bake at 110 °C for 30 sec.

36. Remove the PDMS stamp, leaving the Si on carrier wafer

37. Anneal at 150 °C for 10 min.

38. Anneal at 250 °C for 60 min in N<sub>2</sub> atmosphere.

***Isolating the PIN heaters***

39. Pattern PR (Mask #5: Diode isolation).

40. Etch Si by RIE (50 mTorr, 40 sccm SF<sub>6</sub>, 100 Watt, 3.5 min).

41. Remove PR by acetone.

***Patterning metal to block light***

42. Pattern PR (AZ 4620, 3000 rpm, 30 sec) (Mask #6: Back light blocking metal).
43. Etch PI by RIE (MARCH, 300 mTorr, 150 Watt, 10 min).
44. Wet etch exposed Au/Cr for 54/7 sec.
45. Remove PR by acetone.

***Defining the via hole to the p contact***

46. Spin coat PI (4000 rpm, 30 sec).
47. Anneal at 150°C for 10 min.
48. Anneal at 250°C for 60 min in N<sub>2</sub> atmosphere.
49. Pattern PR (AZ 4620) (Mask #7: P via hole).
50. Etch PI by RIE (MARCH, 300 mTorr, 150 Watt, 10 min).
51. Remove PR by acetone.

***Defining the metal for the p contact***

52. Deposit Cr/Au (5/300 nm) by DC sputtering (AJA International).
53. Pattern PR (AZ 5214) (Mask #8: P metal).
54. Wet etch exposed Au/Cr for 54/7 sec.
55. Remove PR by acetone.

***Defining the via hole to the n contact***

56. Spin coat PI (4000 rpm, 30 sec).
57. Anneal at 150°C for 10 min.
58. Anneal at 250°C for 60 min in N<sub>2</sub> atmosphere.
59. Pattern PR (AZ 4620) (Mask #9: N via hole).
60. Etch PI by RIE (MARCH, 300 mTorr, 150 Watt, 20 min).

61. Remove PR by acetone.

***Defining the metal for the n contact***

62. Deposit Cr/Au (5/300 nm) by DC sputtering (AJA International).

63. Pattern PR (AZ 5214) (Mask #10: N metal).

64. Wet etch exposed Au/Cr for 54/7 sec.

65. Remove PR by acetone.

***Depositing PI encapsulation***

66. Spin coat PI (4000 rpm, 30 sec).

67. Anneal at 150°C for 10 min.

68. Anneal at 250°C for 60 min in N<sub>2</sub> atmosphere.

***Releasing the device***

69. Deposit 150 nm SiO<sub>2</sub> by PECVD.

70. Treat with HMDS for 2 min.

71. Pattern PR (Mask #11: Releasing hole 2).

72. Etch SiO<sub>2</sub> by RIE (50 mTorr, 40:1.2 sccm CF<sub>4</sub>:O<sub>2</sub>, 150 Watt, 8.5 min).

73. Remove PR by acetone.

74. Release device in BOE (6:1).

**3. Fabricating the photodetector array and measuring its characteristics**

Figure S7A shows an exploded schematic illustration of the layout of the Si, metal and PI layers associated with a single unit cell in the photodetector array. The major steps in the fabrication are similar to those for the heater array. Every unit cell in the photodetector array includes a photodiode and blocking diode constructed in a back-to-back configuration to eliminate crosstalk in passive matrix readout. In addition, the light sensitive intrinsic region of

the blocking diode is covered by a layer of Cr/Au to eliminate any response to light. Figure S7B shows the planar structure design of the photodetector. An optical image of the thin photodetector array appears in Fig. S7C. Detailed fabrication steps are as follows.

**Fabrication steps:**

***Defining alignment markers***

1. Clean 1.25  $\mu\text{m}$  SOI wafer with acetone, IPA and DI water.
2. Pattern PR (AZ5214) (Mask #1: Alignment marker).
3. Etch Si by RIE (50 mTorr, 40 sccm SF<sub>6</sub>, 100 Watt, 1 min).
4. Remove PR by acetone and clean by piranha for 10 min.

***Performing p+ doping***

5. Deposit 900 nm SiO<sub>2</sub> by PECVD.
6. Treat with HMDS for 2 min.
7. Pattern PR (Mask #2: P doping).
8. Bake at 110°C for 5 min.
9. Etch SiO<sub>2</sub> in BOE (6:1) for 1.5 min.
10. Remove PR by acetone and clean by piranha for 10 min.
11. Expose to a boron doping source at 1000°C for 30 min.
12. Clean the processed wafer (HF 2 min, piranha 10 min, BOE 1 min).

***Performing n+ doping***

13. Deposit 900 nm SiO<sub>2</sub> by PECVD,
14. Treat with HMDS for 2 min.
15. Pattern PR (Mask #3: N doping).
16. Bake at 110°C for 5 min.

17. Etch SiO<sub>2</sub> in buffered oxide etchant (BOE, 6:1) for 1.5 min.
18. Remove PR by acetone and clean by piranha for 10 min.
19. Expose to a phosphorus doping source at 1000°C for 10 min.
20. Clean the processed wafer (HF 2 min, piranha 10 min, BOE 1 min).

#### ***Releasing top Si from SOI***

21. Pattern PR (AZ 5214) (Mask #4: Releasing hole 1).
22. Etch Si by RIE (50 mTorr, 40 sccm SF<sub>6</sub>, 100 Watt, 3.5 min).
23. Remove PR by acetone and clean by piranha for 10 min.
24. Etch buried oxide layer in concentrated HF for 45 min.
25. Rinse and clean the processed wafer in DI wafer.

#### ***Retrieving the Si film***

26. Bring a 6 mm thick PDMS (weight ratio of base: curing agent=10:1) stamp into contact with the Si.
27. Peel the stamp back to lift the Si film from SOI onto the stamp.

#### ***Preparing the carrier wafer***

28. Spin cast PI (4000 rpm, 30 sec) onto a 3"×2" glass slide
29. Anneal at 150°C for 10 min.
30. Anneal at 250°C for 60 min in N<sub>2</sub> atmosphere.
31. Deposit Cr/Au (5/300 nm) by electron beam evaporation.

#### ***Transfer printing the Si film***

32. Spin coat the carrier wafer with PI (4000 rpm, 30 sec).
33. Bake at 110°C for 30 sec.
34. Bring the stamp with Si film on onto contact with the carrier wafer.

35. Bake 110°C for 30 sec.
36. Retrieve the PDMS stamp, leaving the Si on carrier wafer.
37. Anneal at 150°C for 10 min.
38. Anneal at 250°C for 60 min in N<sub>2</sub> atmosphere.

#### ***Isolating the photodetectors***

39. Pattern PR (Mask #5: Photodetector isolation).
40. Etch Si by RIE (50 mTorr, 40 sccm SF<sub>6</sub>, 100 Watt, 3.5 min).
41. Remove PR by acetone.

#### ***Patterning metal to block light***

42. Pattern PR (AZ 4620, 3000 rpm, 30 sec) (Mask #6: Back light blocking metal).
43. Etch PI by RIE (MARCH, 300 mTorr, 150 Watt, 10 min).
44. Wet etch exposed Au/Cr for 54/7 sec.
45. Remove PR by acetone.

#### ***Defining via 1***

46. Spin coat PI (4000 rpm, 30 sec).
47. Anneal at 150°C for 10 min.
48. Anneal at 250°C for 60 min in a N<sub>2</sub> atmosphere.
49. Pattern PR (AZ 4620) (Mask #7: Via hole 1).
50. Etch PI by RIE (MARCH, 300 mTorr, 150 Watt, 10 min).
51. Remove PR by acetone.

#### ***Depositing and patterning metal 1***

52. Deposit Cr/Au (5/300 nm) by DC sputtering (AJA International).
53. Pattern PR (AZ 5214) (Mask #8: Metal 1).

54. Wet etch exposed Au/Cr for 54/7 sec.

55. Remove PR by acetone.

### ***Patterning via 2***

56. Spin coat PI (4000 rpm, 30 sec).

57. Bake at 150 °C for 10 min.

58. Anneal at 250 °C for 60 min in N<sub>2</sub> atmosphere.

59. Pattern PR (AZ 4620) (Mask #9: Via hole 2).

60. Etch PI by RIE (MARCH, 300 mTorr, 150 Watt, 20 min).

61. Remove PR by acetone.

### ***Depositing and patterning metal 2***

62. Deposit Cr/Au (5/300 nm) by DC sputtering (AJA International).

63. Pattern PR (AZ 5214) (Mask #10: Metal 2).

64. Wet etch exposed Au/Cr for 54/7 sec.

65. Remove PR by acetone.

### ***Depositing PI encapsulation***

66. Spin coat PI (4000 rpm, 30 sec).

67. Anneal at 150 °C for 10 min.

68. Anneal at 250 °C for 60 min in N<sub>2</sub> atmosphere.

### ***Opening the bonding pad***

69. Cover the device with a 2 mm thick piece of PDMS and expose the bonding pad.

70. Etch the unprotected PI (MARCH, 300 mTorr, 150 Watt, 10 min) to expose the bonding pad.

### ***Releasing the device***

71. Deposit 150 nm SiO<sub>2</sub> by PECVD.

72. Treat with HMDS for 2 min.
73. Pattern PR (Mask #11: Releasing hole 2).
74. Etch SiO<sub>2</sub> by RIE (50 mTorr, 40:1.2 sccm CF<sub>4</sub>:O<sub>2</sub>, 150W, 8.5 min).
75. Remove PR by acetone.
76. Release device in BOE (6:1).

#### **4. Fabricating and assembling the complete system**

Assembling the complete system involves multiple steps of functional component fabrication and integration. Detailed fabrication steps are outlined in the following.

##### **Fabrication steps:**

##### ***Bonding the heater array with thin PDMS***

1. Retrieve the thin heater array with a PDMS stamp.
2. Deposit 40 nm SiO<sub>2</sub> by PECVD.
3. Spin coat PDMS (10:1, 500rpm, 1 min) on a glass slide (2''×3'').
4. Bake at 80°C for 10 min.
5. Treat the front surface of the PDMS under a UVO lamp (BHK Inc.) for 5 min.
6. Bond the heater array with the treated PDMS.

##### ***Constructing the artificial leucophor and chromatophore pixels***

7. Deposit Ag (300 nm) for the white background and heat spreading layer by electron beam evaporation.
8. Pattern PR (AZ 5214) (Mask #1: Ag).
9. Etch exposed Ag by wet etchants for 20 sec.
10. Remove PR by acetone.

11. Pattern the thermochromic composite by spin coating, pre-baking, exposing, post-baking and developing.

12. Clean with isopropyl alcohol (IPA) and deionized (DI) water.

***Opening the bonding pad for the heater***

13. Cover the device by a rectangular, ring-shaped piece of PDMS (2 mm thick) with a glass slide on top and expose the bonding pad.

14. Etch the unprotected PI (MARCH, 300 mTorr, 150 Watt, 10 min) to expose the bonding pad.

15. Peel off the PDMS with the heater and color changeable pixel array from the glass slide.

***Bonding the photodetector array***

16. Treat the back surface of the PDMS under a UVO lamp for 5 min.

17. Retrieve the photodetector array with a PDMS stamp.

18. Deposit 40 nm SiO<sub>2</sub> by PECVD.

19. Align and bond the photodetector array to the activated rear surface of the PDMS with all other components on the front side.

**5. Optical system and data acquisition**

Connecting the pins on a custom printed circuit board (PCB) that is interfaced to the devices, with control electronics and software enables background image acquisition, signal processing, and pulse power signal generation. Electronic diagrams for image acquisition are shown in Fig. S7D. The inputs and outputs, i.e. the columns and rows respectively, are interfaced with the control electronics of NI PXIe-6363(National Instruments). The current responses at an applied bias of 3 V were measured for all the pixels in the 16 x 16 array, used to generate the image results of Fig. S8. Three different light intensities ranging from bright, working to complete darkness served to test the detector arrays. A good range of sensitivity is possible for the

photodetecting pixels, from current responses of 1100~1200 nA at the highest brightness to 0.5~3 nA in the dark state, as shown in Fig. 2C. The greyscale image of Fig. S8A represents the normalized photocurrent intensity map during image acquisition, while the binarized image by choosing the cut-off value of 0.25 was achieved as shown in Fig. S8B. The binarized data were used to control the pulse voltages to supply the heaters, thus to induce color change and pattern matching.

The circuit diagram of the heater array is shown in Fig. S5. Instead of directly interfacing the devices with the PXI control electronics, the heaters were powered using the output of a transistor (MCT2EM-ND, Fairchild Semiconductor Corp.) capable of meeting the power requirements. Figure S6 shows the controlling pulse (3 V) from the PXIe-6723 and the power supply pulse (12 V). The voltage directly applied to the heater pixel is 10.5 V, since there is some voltage drop on the two forward biased junctions from the circuit.

## **6. Moving background setup and device testing**

The changeable background, which was used to verify the camouflaging capabilities, consisted of a backlight and a transparency mask. Specifically, diffusive light from an array of light emitting diodes (MB-BL4X4, Metaphase Technologies, Inc., USA) provided a uniform, white light illumination. The plastic transparency masks consist of various black patterns that block the light. Motion of this mask relative to the device system allowed demonstrations of dynamic change of the patterns. The schematic cartoons with various patterns are shown in Fig. 4. The whole setup was built on a stage to allow temperature control, with a set point of  $T_0$ .

## **7. Thermal analysis**

FEM, specifically the continuum element DC3D8 in the ABAQUS software(1), was used to study the temperature distribution in the device. The substrate, made of PI (thickness 9.95  $\mu\text{m}$ ) and PDMS (thickness 100  $\mu\text{m}$ ), was supported by a glass slide (thickness 1100  $\mu\text{m}$ ). As shown in Fig. S16A, the device consists of  $16 \times 16$  pixels on the substrate, where each pixel consists of a layer of composite dye (thickness 65  $\mu\text{m}$ ) and Ag (thickness 0.3  $\mu\text{m}$ ) (Fig. S16B). The pixels have spacing of 100  $\mu\text{m}$ , and in-plane dimensions of  $820 \times 820 \mu\text{m}^2$  with four corners (each  $110 \times 110 \mu\text{m}^2$ ) removed (Fig. S16C). For each pixel, the PI layer underneath contains the (Si) heater and the gold layer with dimensions of  $640 \times 640 \times 1.25 \mu\text{m}^3$  and  $720 \times 720 \times 0.3 \mu\text{m}^3$ , respectively (Fig. S2B). Figures S16 A and C also show Au interconnects between the heaters. The bottom of the glass slide has a constant temperature 40.5  $^\circ\text{C}$ , as in experiments. The entire top surface, and the lateral surfaces of pixels, have natural convection with the coefficient of heat convection of 5  $\text{W}/(\text{m}^2 \cdot \text{K})$  and air temperature of 20  $^\circ\text{C}$ . Figure S16D illustrates the pulsed voltage of  $U_0 = 10.5 \text{ V}$  and duration of  $t_0 = 17.5 \text{ ms}$  in the period of  $T = 280 \text{ ms}$ .

The thermal conductivity, heat capacity, and mass density are 0.2  $\text{W}/(\text{m} \cdot \text{K})$ , 1800  $\text{J}/(\text{kg} \cdot \text{K})$ , and  $1200 \text{ kg}/\text{m}^3$  for thermochromic dye(2, 3); 371  $\text{W}/(\text{m} \cdot \text{K})$ , 235  $\text{J}/(\text{kg} \cdot \text{K})$ , and  $10492 \text{ kg}/\text{m}^3$  for silver(4); 0.52  $\text{W}/(\text{m} \cdot \text{K})$ , 1090  $\text{J}/(\text{kg} \cdot \text{K})$ , and  $1420 \text{ kg}/\text{m}^3$  for PI(5, 6); 160  $\text{W}/(\text{m} \cdot \text{K})$ , 700  $\text{J}/(\text{kg} \cdot \text{K})$ , and  $2329 \text{ kg}/\text{m}^3$  for silicon(7); 317  $\text{W}/(\text{m} \cdot \text{K})$ , 129  $\text{J}/(\text{kg} \cdot \text{K})$ , and  $19280 \text{ kg}/\text{m}^3$  for gold(8, 9); 0.18  $\text{W}/(\text{m} \cdot \text{K})$ , 970  $\text{J}/(\text{kg} \cdot \text{K})$ , and  $1460 \text{ kg}/\text{m}^3$  for PDMS(7); 1.2  $\text{W}/(\text{m} \cdot \text{K})$ , 790  $\text{J}/(\text{kg} \cdot \text{K})$ , and  $2700 \text{ kg}/\text{m}^3$  for glass(10), respectively.

Figure S17A shows the temperature distribution, obtained by FEM, along the plane of the Si heaters ( $x$  direction) as illustrated in Fig. S17B, when all heaters are off except the center one, which receives pulsed power, and the temperature fluctuation is stabilized. The maximum

temperature increase in all heaters without power is only 3% of that in the center heater, which clearly demonstrates that the heat is well confined. Figure S18 shows that, during thermal fluctuation due to pulsed power, the maximum temperature on the surface of the heated pixel ranges from 57 to 65 °C. The temperature along  $z$  direction (normal to the surface) given in Fig. S19 suggests relatively uniform temperature across the thickness of the dye. Figure S20 compares the temperature distributions at the bottom surface of the dye, with and without the Ag layer. With Ag, the temperature is more uniform than that of the case of without Ag layer.

## **8. Mechanical analysis**

This analysis of strains and stresses in the device during bending by FEM upon application of a load along the  $x$  and  $y$  directions is performed. The thermochromic composite dye and PDMS are modeled as three-dimensional solids. The multilayer structures consist of metal, silicon and PI, are modeled as shells. The Young's modulus and Poisson's ratio are 130 GPa and 0.27 for silicon, 78 GPa and 0.44 for Au, 2 MPa and 0.49 for PDMS and 2.5 GPa and 0.34 for PI, respectively. Figure S12B captures the maximum strain in the silicon for bending to different bending radii.

## References

1. ABAQUS Analysis User's Manual V6.9 (2009) (Dassault Systèmes, Pawtucket).
2. Kim TI, *et al.* (2012) High-efficiency, microscale GaN light-emitting diodes and their thermal properties on unusual substrates. *Small* 8(11):1643-1649.
3. Solano B, Rolt S, & Wood D (2008) Thermal and mechanical analysis of an SU8 polymeric actuator using infrared thermography. *Proc Inst Mech Eng C J Mech Eng Sci* 222(1):73-86.
4. Smith DR & Fickett FR (1995) Low-temperature properties of silver. *J Rre Natl Inst Stan* 100(2):119-171.
5. Dhorajiya AP, *et al.* (2010) Finite element thermal/mechanical analysis of transmission laser microjoining of titanium and polyimide. *ASME J Eng Mater Technol* 132(1) 011004.
6. Hu ZL, Carlberg B, Yue C, Guo XM, & Liu JH (2009) Modeling of nanostructured polymer-metal composite for thermal interface material applications. in *2009 International Conference on Electronic Packaging Technology & High Density Packaging*, pp 405-408.
7. Li R, *et al.* (2012) Thermo-mechanical modeling of laser-driven non-contact transfer printing: two-dimensional analysis. *Soft Matter* 8(27):7122-7127.
8. Bourgoin JP, Allogho GG, & Hache A (2010) Thermal conduction in thin films measured by optical surface thermal lensing. *J Appl Phys* 108(7):073520.
9. J. F. Shackelford WA (2001) *CRC Materials Science and Engineering Handbook* (CRC Press LLC).

10. Tari M, *et al.* (2003) A high voltage insulating system with increased thermal conductivity for turbo generators. *Proceedings: Electrical Insulation Conference and Electrical Manufacturing & Coil Winding Technology Conference*, pp 613-617.

### **Supplementary Movie Legends**

Movie S1. Experimental thermal movie of camouflaging of a digital pattern “O”.

Movie S2. FEM thermal movie of camouflaging of a digital pattern “O”.

Movie S3. Movie of dynamic, adaptive pattern recognition and color camouflaging against a moving square background. The video is sped up by 3 times.

Movie S4. Movie of dynamic, adaptive pattern recognition and color camouflaging on a changing background. The video is sped up by 3 times.

### **Supplementary Figure Legends**

Figure S1. (A) Optical image of the black thermochromic slurry at room temperature,  $\sim 22^{\circ}\text{C}$ . (B) Optical image of the slurry at  $47^{\circ}\text{C}$ . At this temperature, the slurry is transparent, thereby a background picture underneath is visible. (C) SEM image of an array of photopatterned thermochromic pixels. (D) SEM image of the top surface of a patterned pixel. (E) Optical image of the pixel arrays ( $16\times 16$ ) at room temperature of  $22^{\circ}\text{C}$ . (F) Optical image of the arrays ( $16\times 16$ ) at  $47^{\circ}\text{C}$ .

Figure S2. (A) Exploded schematic illustration of the layout of the Si, metal, and PI layers of a single pixel in the heater array. (B) Optical image of the Si diode. The dark dots represent the releasing holes etched through the Si. (C) Optical image of the heater array. (D) Thermal image of the array with one pixel activated. The heat is mostly confined within the area of the activated heater, with minimal changes in neighboring pixels. The background temperature was set to  $30^{\circ}\text{C}$ .

Figure S3. Schematic illustration of the major steps for fabricating flexible devices based on Si nanomembranes. (A) Preparing the device elements by selective doping. (B) Opening holes and undercut etching in concentrated HF. (C) Retrieving the Si from the SOI wafer using a PDMS stamp. (D) Printing the Si onto a glass substrate with a thin layer of PI. (E) Peeling away the stamp to leave the Si on the glass. (F) Patterning the Si and completing the metallization and passivation steps. (G) Releasing the flexible device from the glass.

Figure S4. (A) Optical images of a diode heater with P<sup>+</sup> and N<sup>+</sup> doping regions on an SOI wafer. (B) Optical image of a 1.25 μm thick Si membrane on a PDMS stamp. (C) Optical image of the Si membrane transfer printed onto a glass substrate which was coated with PI. (D) Optical image of a flexible array of diode heater held by a tweezer.

Figure S5. Schematic circuit diagram of a heater array and its external circuits.

Figure S6. Images of representative pulse signals. (A) The green curve is the control signal generated with a program created in Labview. The yellow curve is the output pulse applied to the heater. (B) Magnified image of both curves.

Figure S7. (A) Exploded schematic illustration of the layout of the Si, metal, and PI layers of a single pixel in the photodetector array. (B) Schematic illustration of the photodiode and blocking diode. (C) Optical image of the thin flexible photodetector array folded on a glass slide. (D) Schematic circuit diagram of the photodetector array.

Figure S8. (A) Normalized photocurrent intensity map associated with a digital pattern in the geometry of the text “UIUC MRL”. (B) Corresponding binarized intensity map.

Figure S9. Schematic steps for assembling the entire system. (A) Schematic illustration of a unit cell of the heater array and a thin PDMS substrate, prior to bonding. (B) Illustration of the bonded device. (C) Illustration of the Ag pixel fabricated on the device. (D) Illustration of a unit cell of the thermochromic pixel on top of the Ag pixel and the photodetector to be bonded together. (E) Illustration of the integrated system.

Figure S10. (A) Optical image of the heater array on a PDMS substrate. (B) Optical image of the Ag pixels fabricated on the heater array. (C) Optical image of the heater array and Ag pixels viewed from the backside.

Figure S11. Optical image of the device with ACF cable and custom made PCB with pin connectors.

Figure S12. (A) FEM model of the system, showing a  $5 \times 5$  array. (B) FEM results of the maximum strain in the Si within the device at different bending radii. The red dots are the results for bending along  $x$  axis. The blue dots are the results for bending along  $y$  axis.

Figure S13. (A-H) IR images of the device when one pixel is actuated, as the actuation voltage increases from 5.5 V to 12.5 V, with an increment of 1 V.

Figure S14. (A-D) IR images of the device when 8 pixels (digital pattern of “o”) are actuated, as the actuation voltage increases from 8.5V to 11.5V, with the increment of 1V.

Figure S15. (A) IR image of the heater array with one pixel activated at 10.5V. The arrow points to the geometrical center of the pixel. (B) Temperature fluctuation at the center of the pixel. The power was turned on and off at 11 s and 41 s, respectively. (C) Temperature information during the period of 20~30 s, as highlighted by the red dotted rectangular in (B).

Figure S16. (A) FEM model for the thermal analysis. (B) Cross-sectional (front) view of the pixel with the key dimensions. (C) Top view of the pixels. (D) Schematic pulse input for the FEM simulation.

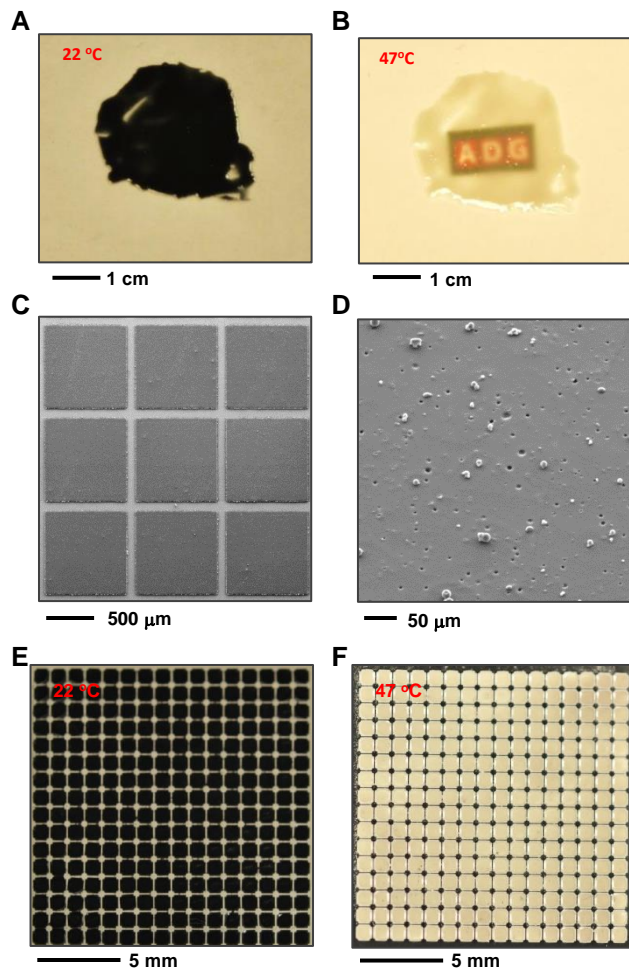
Figure S17. (A) FEM results of the temperature within the layer of the Si heater arrays. The red curve shows the maximum temperature, and the black curve represents the minimum temperature. The results clearly show good heat confinement within the region of the activated pixel. (B) Schematic cross-sectional view of the heater layer.

Figure S18. (A) FEM results of the temperature along the  $x$  axis of the pixel. The black curve shows the maximum temperature, and the red curve represents the minimum temperature. (B) Schematic cross-section view of the heater.

Figure S19. (A) FEM results of the temperature across the thickness of the device. The black curve shows the maximum temperature, and the red curve represents the minimum temperature.

(B) Schematic cross-sectional view of the heater pixel.

Figure S20. (A) FEM results of the temperature along the  $x$  axis of the pixel for the cases with and without Ag heat spreading layer. The black curve shows the maximum temperature with the Ag, and the red curve shows the maximum temperature without Ag. The temperature is more uniform across the whole pixel with Ag. (B) Schematic cross-sectional view of the heater pixel.



**Figure S1**

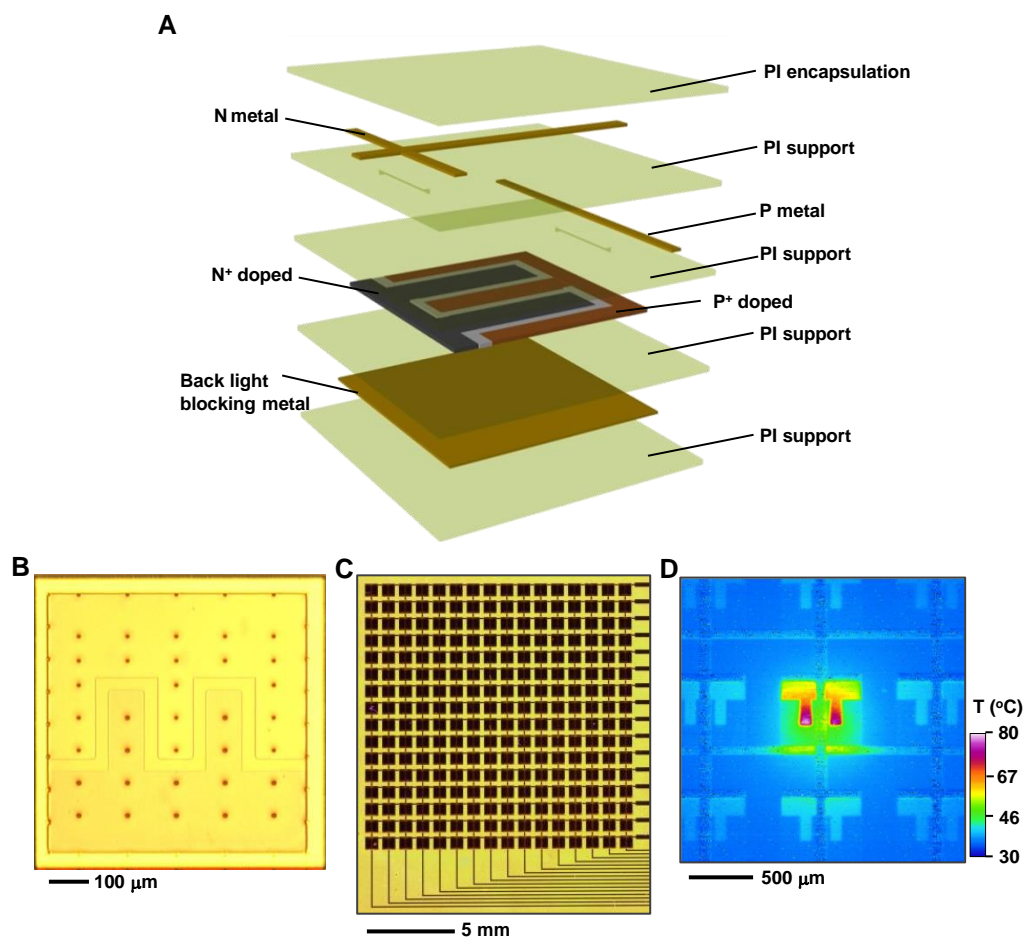


**Figure S2**

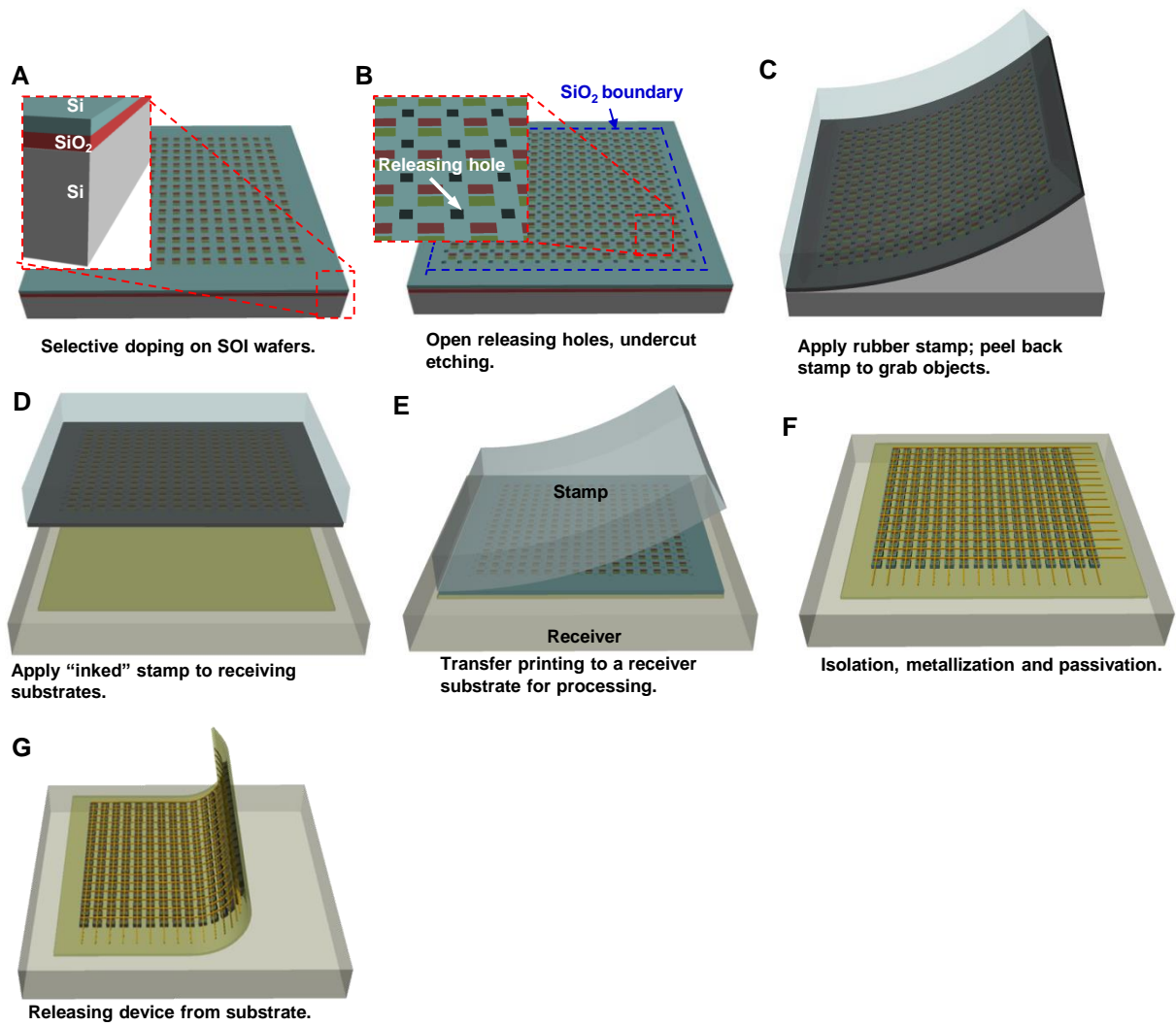


**Figure S3**

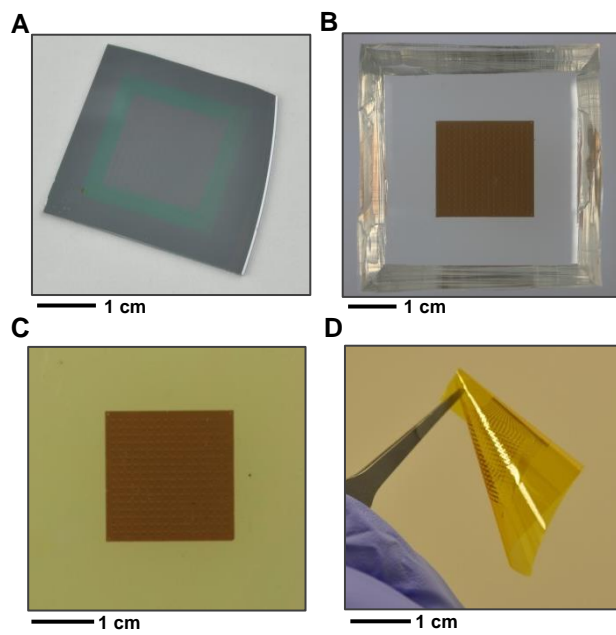


**Figure S4**

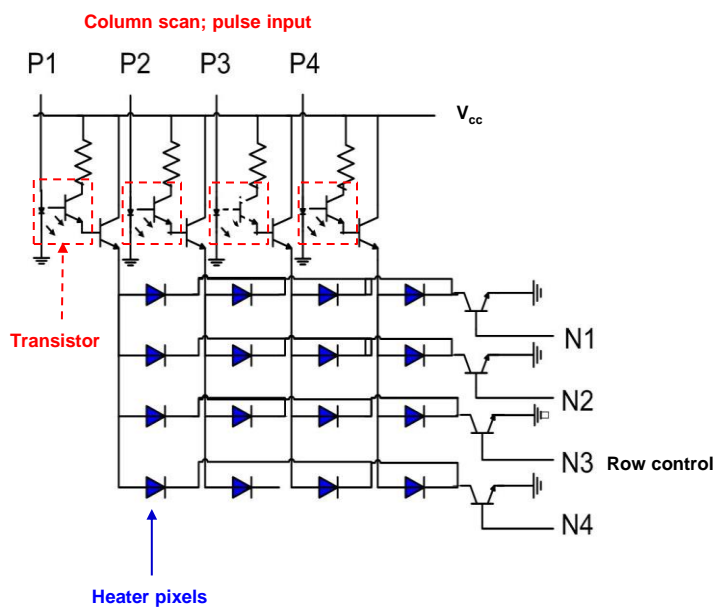
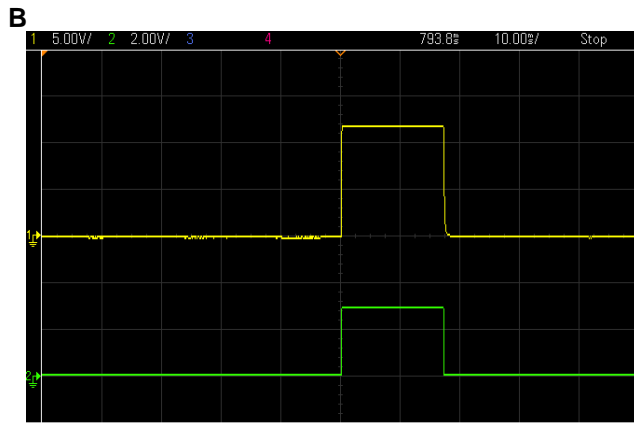
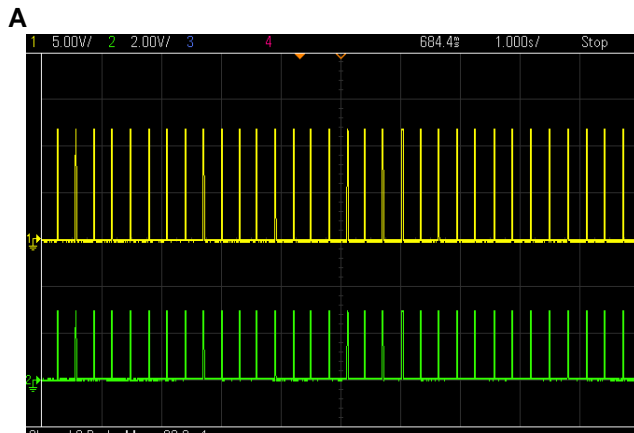
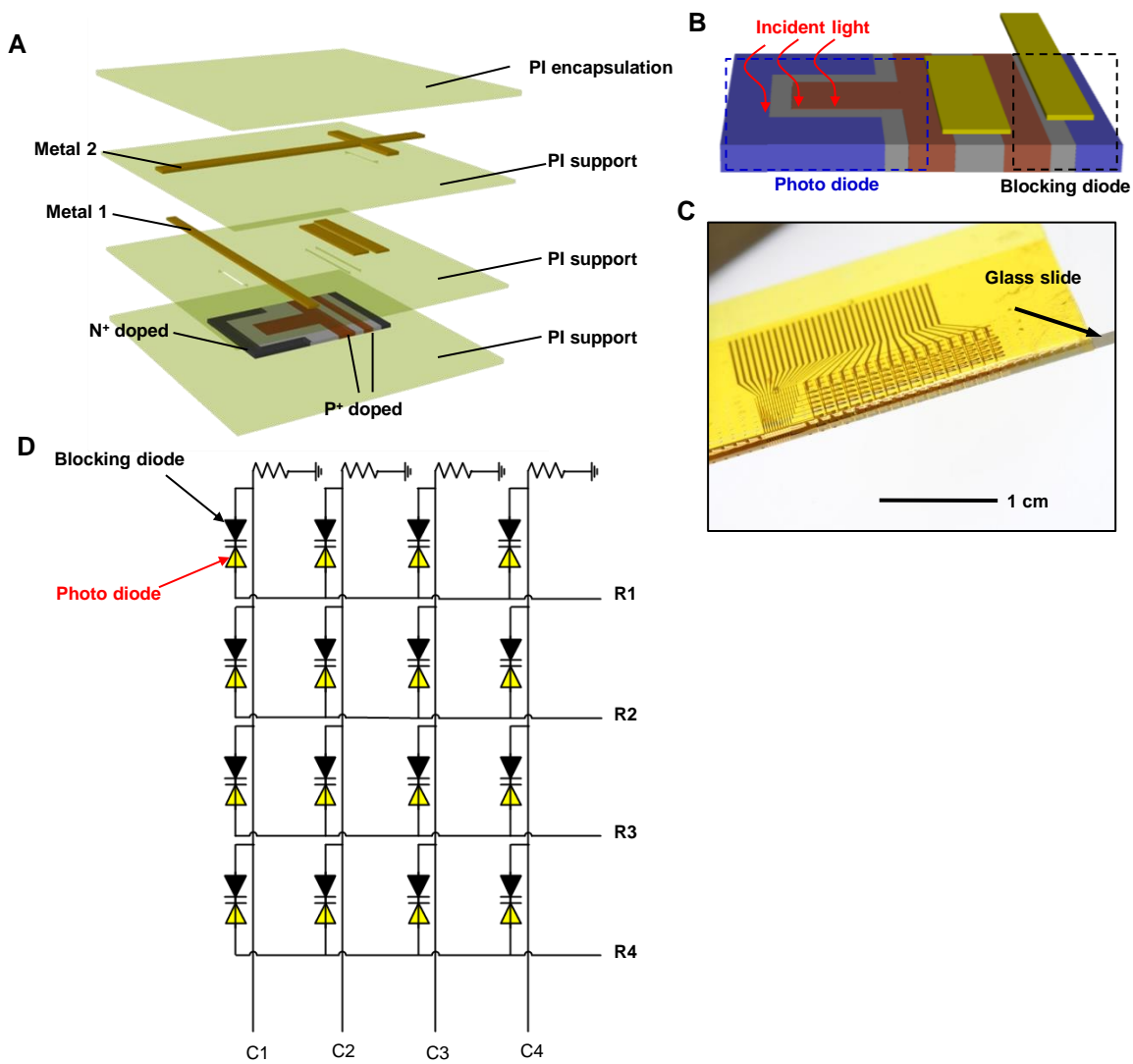


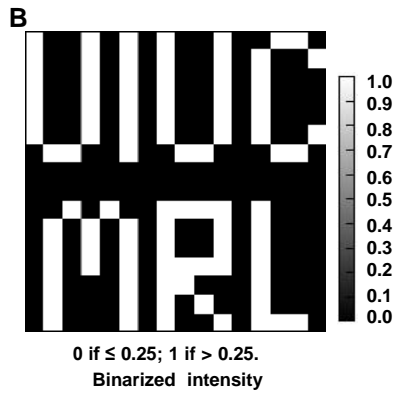
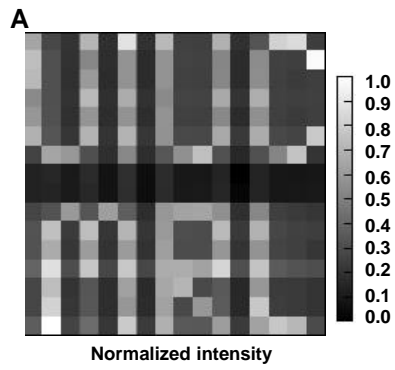
Figure S5



**Figure S6**



**Figure S7**



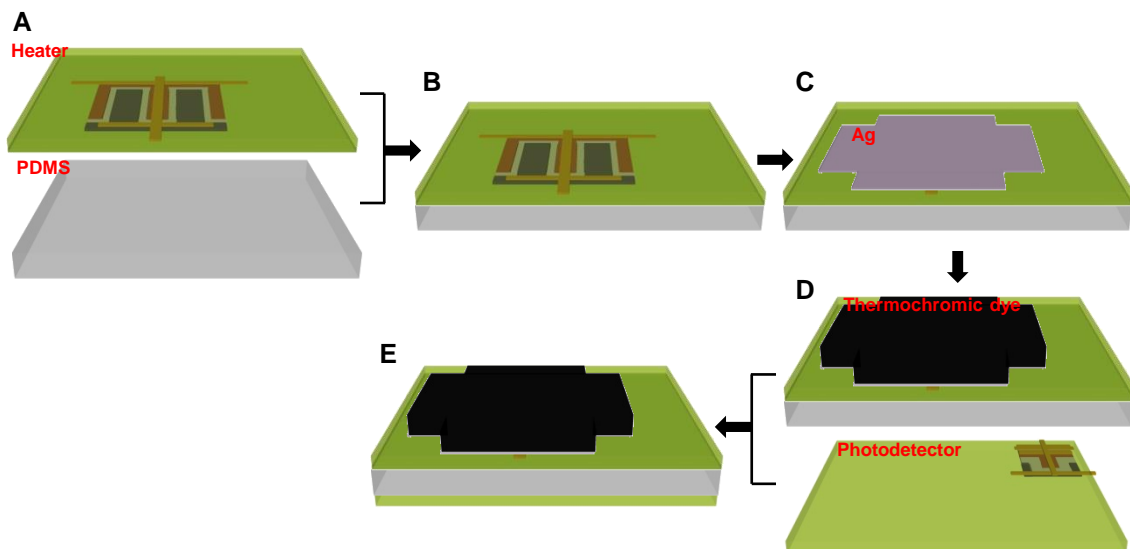
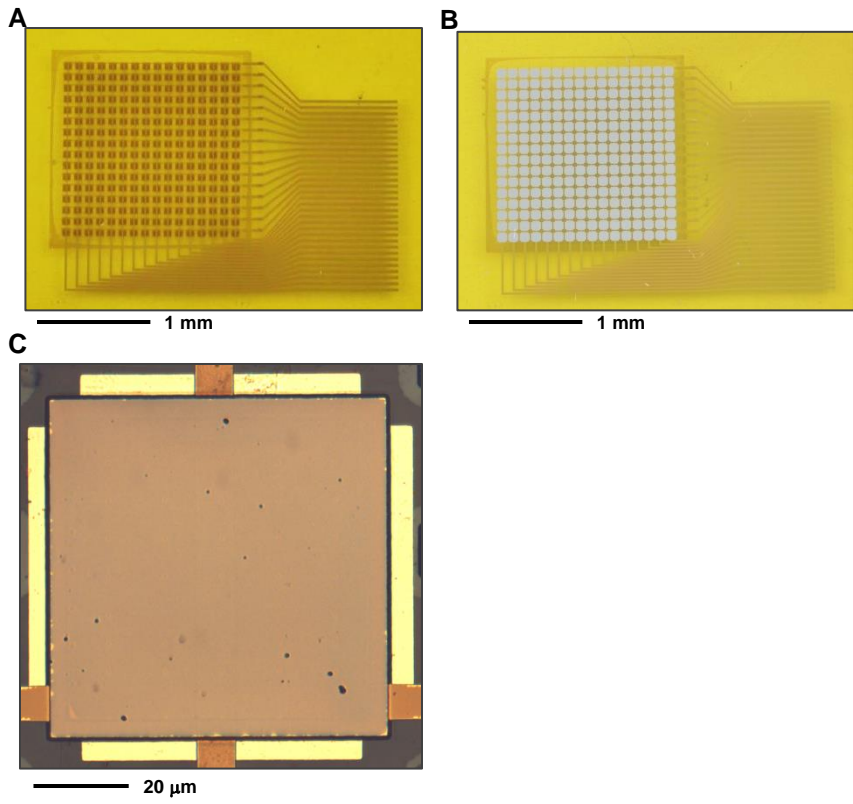
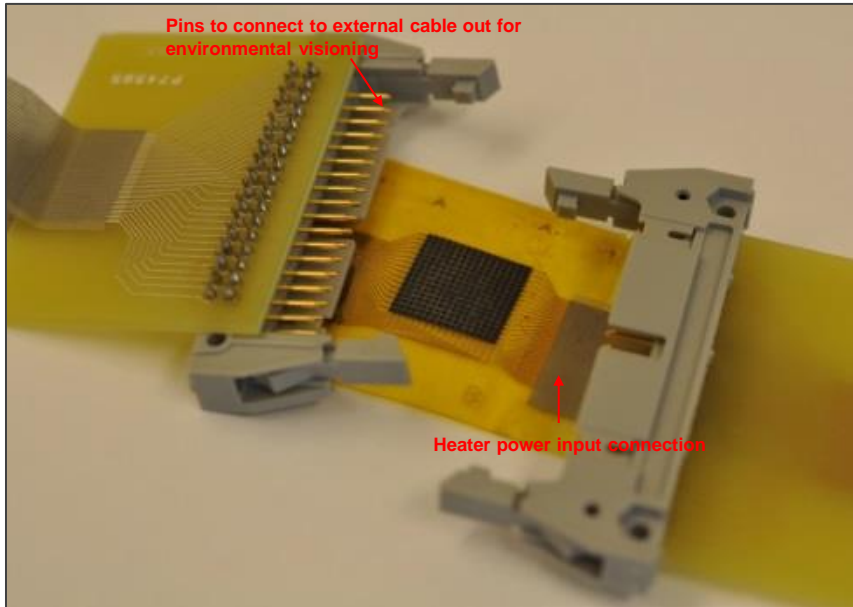


Figure S9



**Figure S10**



1 cm

**Figure S11**

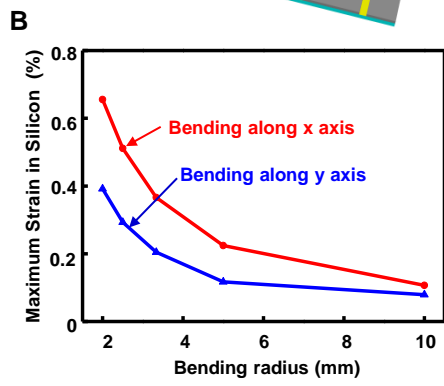
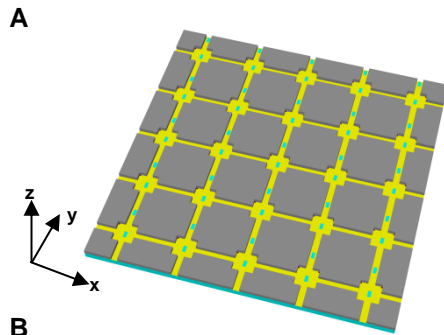


**Figure S12**

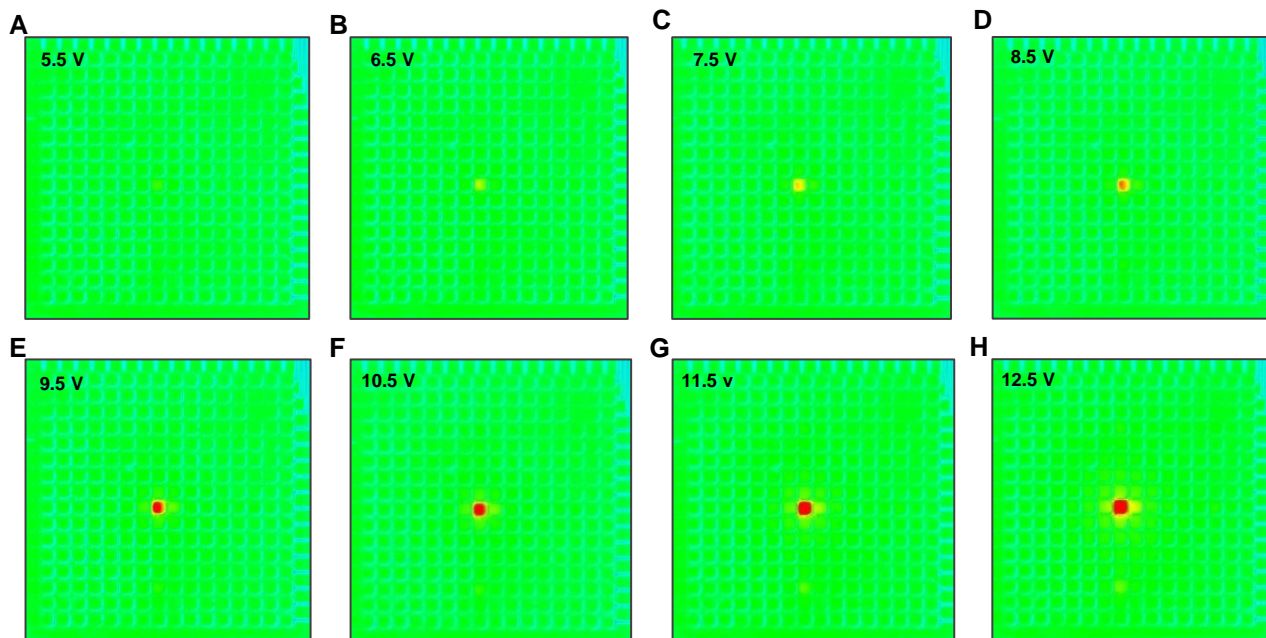


Figure S13

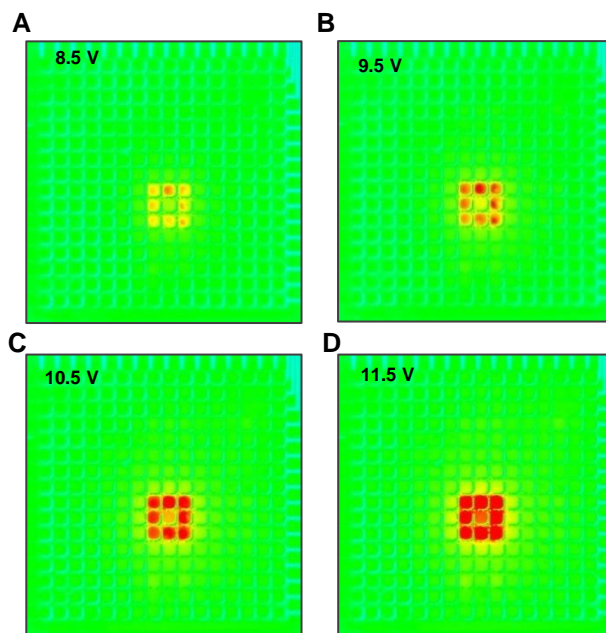
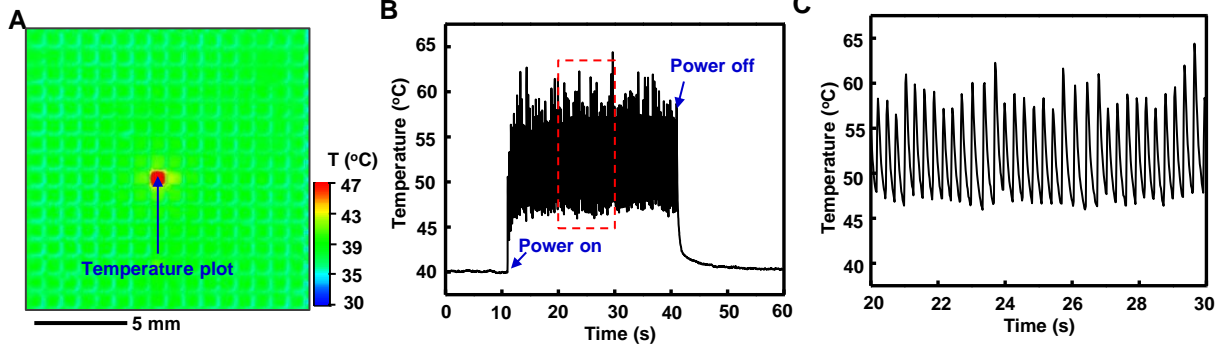


Figure S14



**Figure S15**

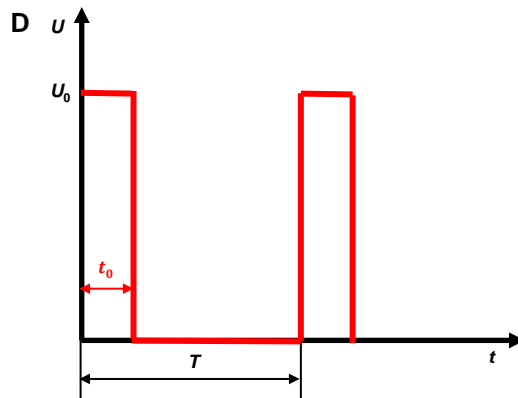
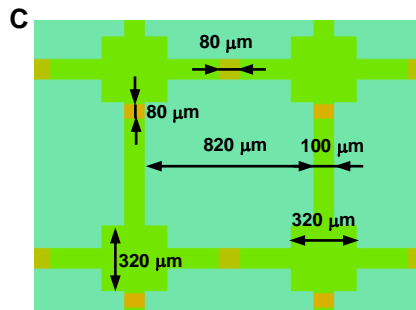
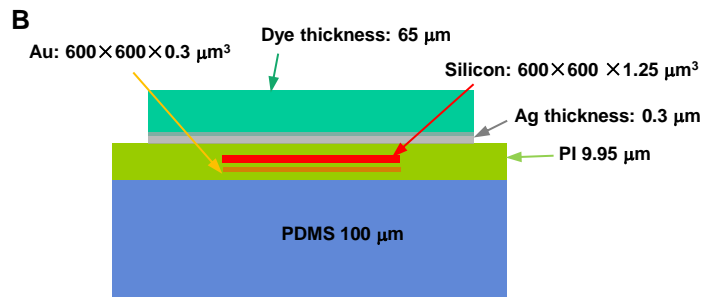
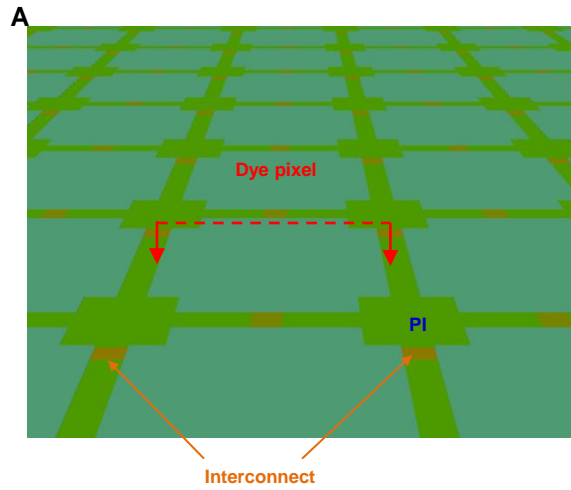


Figure S16

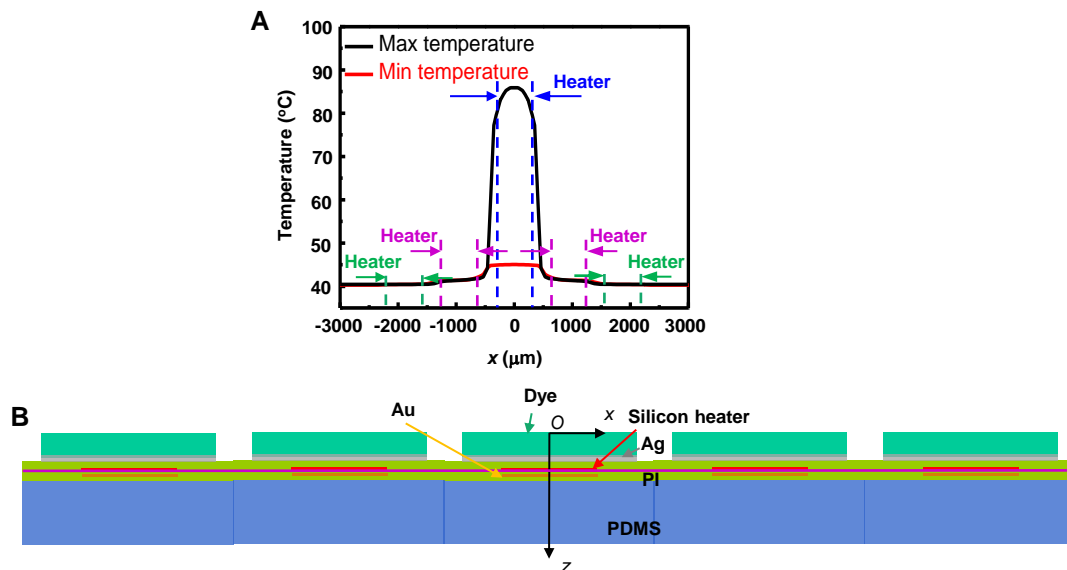
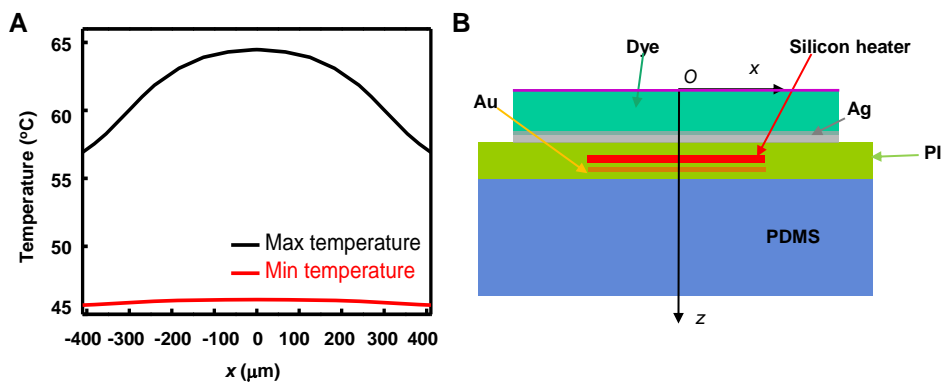
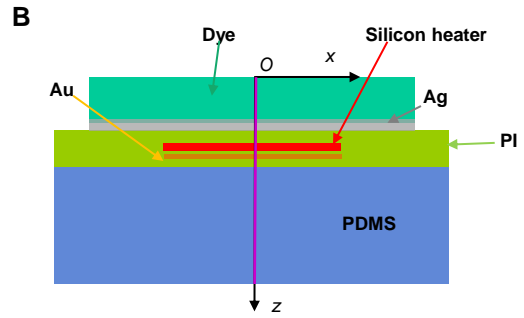
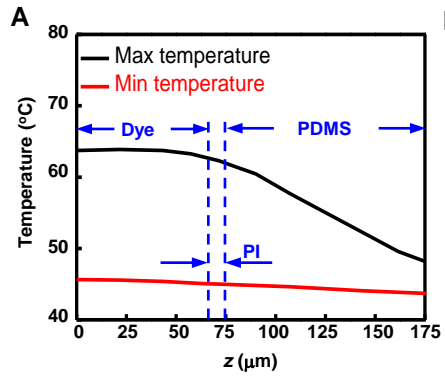


Figure S17



**Figure S18**



**Figure S19**

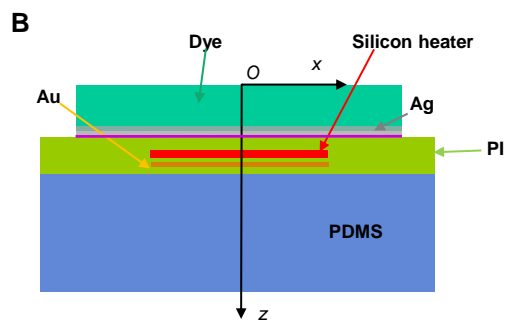
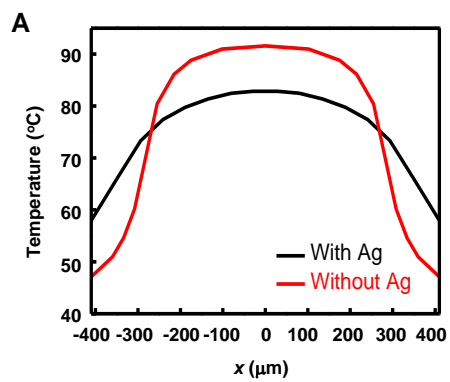
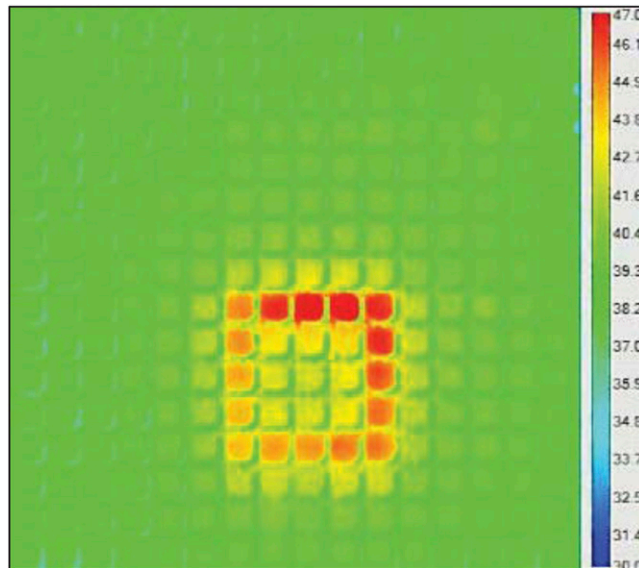


**Figure S20**

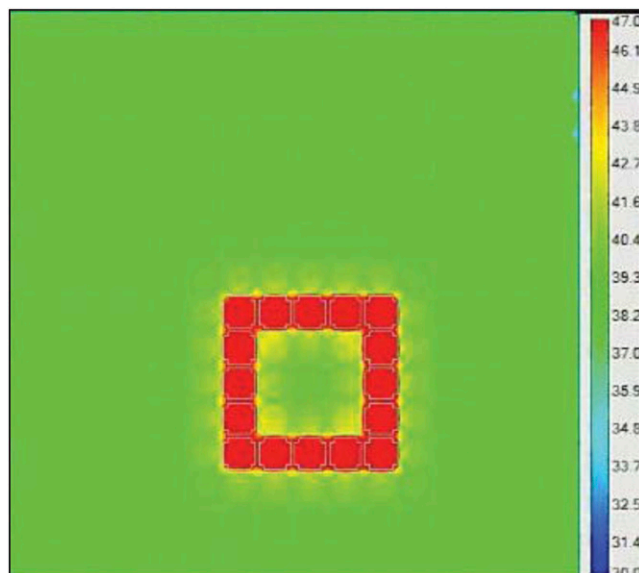
# Supporting Information

Yu et al. 10.1073/pnas.1410494111



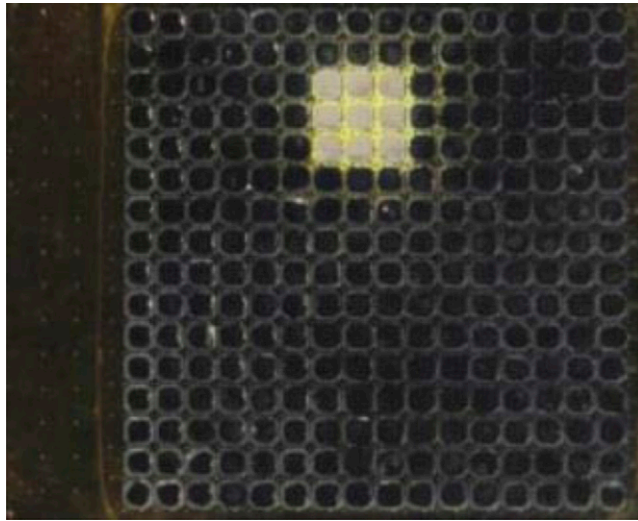
Movie S1. Experimental thermal movie of camouflaging of a digital pattern "O."

[Movie S1](#)



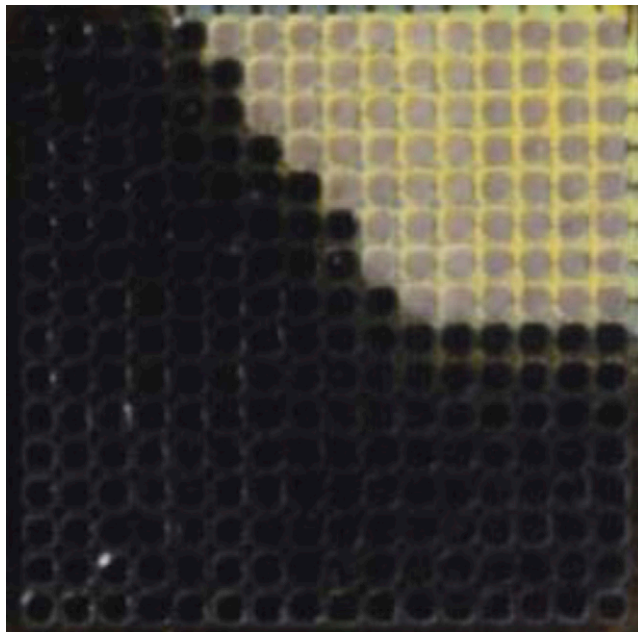
Movie S2. FEM thermal movie of camouflaging of a digital pattern "O."

[Movie S2](#)



**Movie S3.** Movie of dynamic, adaptive pattern recognition and color camouflaging against a moving square background. The video is sped up by three times.

[Movie S3](#)



**Movie S4.** Movie of dynamic, adaptive pattern recognition and color camouflaging on a changing background. The video is sped up by three times.

[Movie S4](#)

## Other Supporting Information Files

[SI Appendix \(PDF\)](#)